

# A systematic approach to assessing the sensitivity and vulnerability of water availability to climate change in Europe

Martina Weiß<sup>1</sup> and Joseph Alcamo<sup>1</sup>

Received 13 August 2009; revised 1 October 2010; accepted 22 October 2010; published 26 February 2011.

[1] Making use of ensemble climate modeling systems and multimodel simulations of climate projections calls for a systematic approach in impact studies. In this study the response surface method is introduced to systematically, consistently, and objectively examine impacts of climate change on water availability, subject to selected impact thresholds. The response surface hereby represents the sensitivity of water availability to a broad range of possible climatic change, onto which vulnerability thresholds are superimposed. Their exceedance is assessed by additionally superimposing climate change projections onto the surface. With this method, 18 European river basins are ranked according to their sensitivity to climate change (analyzing the response surface itself). The use of climate change projections from six regional climate models for the year 2100 under the Intergovernmental Panel on Climate Change A1B emissions scenario in combination with societal vulnerability thresholds then enables a vulnerability ranking of these basins. Overall, a strong climate sensitivity of the Nordic basins is found on the basis of their mainly snow-dominated flow regime. When looking at the vulnerability, however, southern European basins together with some central European basins are highest in the ranking because of the violation of both low flow and water stress thresholds.

**Citation:** Weiß, M., and J. Alcamo (2011), A systematic approach to assessing the sensitivity and vulnerability of water availability to climate change in Europe, *Water Resour. Res.*, 47, W02549, doi:10.1029/2009WR008516.

## 1. Introduction

[2] Examining climate change and its effects now has a history of almost three decades. A wide variety of scenarios [e.g., Arnell and Liu, 2001; Carpenter *et al.*, 2005; United Nations Environment Programme (UNEP), 2007] has since been developed to qualify and quantify required model drivers and set the context for carrying out climate change scenario analysis. Profound advances have been made in both climate models and impact models, generating complex projections of potential environmental and socioeconomic consequences and setting the scene in the planning of adaptation and mitigation strategies.

[3] Impact analysis has hereby mostly followed the conventional way of a cause-effect analysis [Bruckner *et al.*, 1999]. On the basis of a consistent set of socioeconomic drivers, emission paths for various greenhouse gases are developed, which are then used to simulate future climates that constitute the basis for impact analyses [e.g., Intergovernmental Panel on Climate Change (IPCC), 2000]. Although including largely divergent drivers, this type of scenario analysis only provides insight into a finite, and often small, number of possible consequences along rigid pathways at a certain time in the future.

[4] Climate data available to drive impact models have increased notably: The urge to address climate model sensi-

tivities, model imperfections, and inherent uncertainties in the climate modeling process has recently resulted in developing ensemble climate model systems consisting of a number of models that lead to a wide range of projected changes [Collins, 2007]. Impact analysis with projected ranges of climate change, however, can become cumbersome, especially when carried out with a complex impact model in the cause-effect analysis mode, as impact model simulations have to be carried out for each of the climate change projections in order to identify the range of possible impact.

[5] For the applicability of impact analysis results, for example, providing scientific support for policy makers, the absolute value of an impact might not be of much interest. As for the planning of adaptation and mitigation strategies, it is rather the sensitivity of a system toward change that is relevant along with how close the system moves toward thresholds of unacceptable limits.

[6] For these reasons, this study introduces a systematic sensitivity analysis of water availability to climate change that is applied to 18 European river basins. Response surfaces are created for each basin, showing the response of water availability to a change in average annual climate, for changes of temperature in the range of  $-1^{\circ}\text{C}$  to  $+6^{\circ}\text{C}$  of current conditions combined with changes in precipitation in the range of  $-40\%$  to  $+100\%$  of current conditions. Different aspects of the response are then analyzed, covering the nature of the system itself, as well as human impact on the system. The study concludes with a vulnerability ranking subjective to the chosen thresholds, for the first time, comparing a great number of basins throughout Europe under the conditions of a future climate cycle as projected by six

<sup>1</sup>Center for Environmental Systems Research, Kassel, Germany

different regional climate models (RCMs) for the year 2100 under the A1B emissions scenario.

## 2. Materials and Methods

### 2.1. Modeling Water Availability

[7] The sensitivity of the water availability to climate change is assessed by means of one of the current state-of-the-art integrated global hydrological models, WaterGAP [Alcamo *et al.*, 2003a; Döll *et al.*, 2003], which has been applied in a wide range of scenario studies, including, e.g., IPCC assessment reports [Arnell and Liu, 2001], Global Environment Outlook Assessments 3 and 4 [UNEP, 2002, 2007], and the Millennium Ecosystem Assessment [Alcamo *et al.*, 2005; Carpenter *et al.*, 2005]. In the present study, model version 2.2 was used with settings as specified below.

[8] Simulations of river discharge are forced by a 30 year period of monthly climate time series from the Climatic Research Unit (CRU) gridded data set of monthly precipitation, air temperature, cloud cover, and wet day frequency (CRU TS 2.1 [Mitchell and Jones, 2005]). These are disaggregated within the model to daily values, e.g., for temperature by applying a cubic spline interpolation and for precipitation based on a first-order Markov chain model of daily precipitation. Further, a range of independent data was used to parameterize land surface characteristics such as the spatial distribution of vegetation, topography, soil types, land use, groundwater, and surface water bodies.

[9] In each grid cell ( $0.5^\circ \times 0.5^\circ$  geographical latitude and longitude) the daily vertical water balance is calculated, quantifying each of its components' actual evapotranspiration, interception, groundwater storage, and surface as well as subsurface runoff. On the basis of climate input, actual evapotranspiration is derived from potential evaporation using a modified Priestley-Taylor approach under the consideration of different climate zones in combination with canopy and soil water balances.

[10] Potential evaporation hereby determines the rate at which water can evaporate, whereby this rate is climate zone dependent. Currently, 12 climate zones are differentiated on the basis of the Köppen-Geiger classification considering vegetation, temperature, and precipitation (M. Weiß *et al.*, Regionalization of the Priestley-Taylor coefficient for use in global hydrological modeling, submitted to *Hydrological Processes*, 2009). Actual evapotranspiration takes evaporation rate into account and further depends on the level of crown and soil water storage. The level of crown moisture saturation determines the fraction of incoming precipitation that directly evaporates without reaching the soil. Maximum canopy storage is calculated as a function of the leaf area index. Development of the leaf area over the year follows a growing function based on precipitation and temperature, whereby 16 vegetation classes are differentiated. Through-fall, hereafter termed effective precipitation, can accumulate actual soil moisture until saturation. Maximum soil water capacity results from the depth of the effective root zone and specific water capacity of the particular soil. A runoff coefficient  $\gamma$  determines the contribution of effective precipitation to an increase of soil moisture storage and to runoff [Bergström, 1995]. If  $\gamma$  equals 1, the contribution to runoff is small for dry soils and increases linearly with increasing soil wetness. A  $\gamma < 1$  increases the runoff response for low

soil wetness nonlinearly, while a  $\gamma > 1$  decreases the runoff response for low soil wetness nonlinearly. The value of  $\gamma$  is parameterized for each basin using measured annual streamflow values, representing basin-specific hydrogeologic and hydromorphologic conditions.

[11] If temperature falls below  $0^\circ\text{C}$ , precipitation is stored as snow. Snow dynamics are modeled at higher resolution, taking into account subgrid variability of elevation and temperature for optimized snow cover and melting process representations on the basis of a land-cover-dependent degree-day factor. Snowmelt increases effective precipitation in a grid cell.

[12] Runoff from land areas is divided into surface runoff and groundwater recharge on the basis of information from cell-specific slope characteristics, soil texture, hydrogeology, and the presence of permafrost and glaciers. Within a cell it passes various storage areas, e.g., groundwater storage, lakes, reservoirs, wetlands, and rivers, with different residence times according to the Global Lake and Wetland Database [Lehner and Döll, 2004]. Excess water is routed to the adjacent grid cell following a global drainage direction map [Döll and Lehner, 2002], unless the cell represents a sink or coastline.

[13] In this study, water availability is defined as the total renewable water resource. River discharge (synonymous with streamflow) is defined as water availability reduced by anthropogenic consumptive uses.

### 2.2. Modeling Anthropogenic Water Use

[14] Time series of consumptive uses are computed for the domestic, industrial, and agricultural sectors. The domestic sector includes municipal and household uses; the industrial sector is subdivided into electricity production and manufacturing facilities; the agricultural sector is subdivided into irrigation and livestock uses [Alcamo *et al.*, 2005].

[15] Time series of irrigation water uses are calculated as a function of climate, extent of irrigated area [Siebert *et al.*, 2005], cropping intensity, and crop type with a 30 arc min grid cell resolution. Evapotranspiration is crop specific and depends on the growing stage of the crop.

[16] Time series of livestock water uses are calculated by multiplying stock numbers per grid cell with stock-specific water demands. The model currently distinguishes 12 animal species: buffalo, dairy cattle, nondairy cattle, camels, chicken, ducks, geese, goats, pigs, sheep, turkey, and horses. Absolute stock numbers per grid cell have been derived on the basis of literature research and were scaled to meet national and subnational statistics, [e.g. Wint and Robinson 2007].

[17] In the domestic and manufacturing sectors, modeled water needs depend on structural and technologic conditions. The structure of water uses considers the combination of water use activities and habits within a sector. Technology directly affects the degree of water efficiency, which is usually higher in industrialized countries. The domestic sector includes household use, small businesses, and other municipal water use. Water use in the domestic sector is based on gross domestic product (GDP) and population density. For the manufacturing sector, a function of gross value added and GDP is applied.

[18] Water use for electricity production mainly results from the need for cooling water. The amount of water

required depends strongly on the cooling system and thermal power plant type. The model currently distinguishes four plant types and three cooling types. Water uses are allocated to the respective grid cell on the basis of the location of power plants.

### 2.3. Model Calibration

[19] In order to meaningfully compare modeled and measured streamflow, limitations in using gauged data for both precipitation and streamflow and a probable mismatch between the two have to be considered. Major sources of uncertainty in gauged precipitation data are, e.g., the difference in instruments, and measuring biases under certain climatic and topographic conditions [Adam *et al.*, 2006]. Similarly, uncertainty in measured streamflow data arises because of difficulties in attributing exact gauge locations, unexplainable mismatches between upstream and downstream measurements and measuring errors, or incomplete information on river regulation, etc.

[20] Therefore, a runoff-correction factor is used, which is defined as the ratio between long-term average measured and modeled discharge. A runoff correction factor is used only in 10 out of the 18 modeled basins. For the Danube, Thames, Seine, Po, and Duoro, this runoff correction decreases runoff by 8%–15%. For the Angerman, Lule, Glomma, and Vaernan Goeta, runoff increases by 10%–20% as a result of the correction factor; for the Kemijoki it increases by 30%. The values of this correction factor are well within the range of precipitation uncertainty and its impact on streamflow simulation generally found in other studies [Fekete *et al.*, 2004; Ungersböck *et al.*, 2001; Yang *et al.*, 2005]. For example, bias correction of precipitation gauge records increased modeled streamflow by 5%–25% in northern latitudes, as shown by Tian *et al.* [2007].

### 2.4. Model Validation

[21] WaterGAP simulations of river discharge have been extensively validated to the constantly updated database of measured discharges from the *Global Runoff Data Centre* [2008], which currently includes 1235 stations worldwide (up from 724 stations in earlier publications [e.g., Alcamo *et al.*, 2003a]).

[22] In Figure 1, four examples of modeled versus observed streamflows are given that roughly cover the climatic range of Europe. To evaluate the agreement between modeled and measured discharge, the following efficiency indicators are calculated:

$$R^2 = \left( \frac{\sum (Q_{\text{mod}} - \bar{Q}_{\text{mod}})(Q_{\text{obs}} - \bar{Q}_{\text{obs}})}{\sqrt{\sum (Q_{\text{mod}} - \bar{Q}_{\text{mod}})^2 \sum (Q_{\text{obs}} - \bar{Q}_{\text{obs}})^2}} \right)^2 [-], \quad (1)$$

$$\text{bias} = \frac{\sum (Q_{\text{obs}} - Q_{\text{mod}})}{n} [\text{m}^3/\text{s}], \quad (2)$$

$$\text{NSE} = 1 - \frac{\sum (Q_{\text{mod}} - Q_{\text{obs}})^2}{\sum (Q_{\text{obs}} - \bar{Q}_{\text{obs}})^2} [-], \quad (3)$$

where  $R^2$  is the coefficient of determination, bias the systematic error and NSE the Nash-Sutcliffe efficiency [Nash and Sutcliffe, 1970].  $\bar{Q}_{\text{mod}}$  is the mean monthly modeled

streamflow,  $Q_{\text{obs}}$  is the mean monthly observed streamflow,  $\bar{Q}_{\text{obs}}$  is the average of the mean monthly observed, modeled streamflow values, respectively. A value of 1.0 for  $R^2$  indicates that all variance in the model can be explained by the variance in measured data. Bias is defined as the difference of observed and modeled streamflow divided by the number data pairs of observed and modeled flow. A value of zero represents a perfect simulation of the observed flow. Negative and positive values represent an average overestimation and underestimation of the flow over the simulation period, respectively. Since bias is given as an absolute value, it should be compared to mean and maximum flow of a particular catchment rather than between different catchments. A NSE of 1.0 indicates that the model results correspond to observations; possible values of NSE may include a range between  $-\infty$  and 1.

[23] As can be seen from Figure 1, the WaterGAP model captures well magnitude, timing, and the seasonal cycle of the simulated discharges.  $R^2$  and NSE in Table 1 are in the ranges of 0.72–0.83, and 0.69–0.83, respectively. The bias shows a small underestimation of streamflow for the Glomma and overestimation for the Tagus. These, however, are within 5% and 7% relative to the mean streamflow, and therefore within acceptable ranges. It is therefore concluded that the model is able to reproduce the streamflow hydrographs adequately and is suitable for use in this study.

### 2.5. Climate Impact Response Surfaces

[24] In this study, the response surface method is introduced to climate change impact assessments as a tool that reduces the analysis of the response of a system to two main triggers. This reduction, in turn, then allows an outspread analysis of the response to a wide variation in these two triggers. With their combination, these responses form a response surface. By superimposing vulnerability thresholds, societal windows of tolerance can be marked onto that response surface. The exceedance of these thresholds, i.e., the movement of the system outside tolerable conditions, is then assessed by further superimposing climate change projections onto the surface, which indicates the positioning of a possible future on the basis of scenario conditions compared to present conditions on this surface. In the following, this is described in more detail.

[25] The response surface method is adopted from system sciences, where it is used as a standard approach to analyze system behavior and optimize operating conditions at a large scale [Box and Wilson, 1951; Box and Draper, 1959; Cornell, 1987; Hill and Hunter, 1966; Myers *et al.*, 1989; Myers, 1999]. Applications to the field of climate change impact analysis have, to our knowledge, mainly been carried out under the Integrated Assessment of Climate Protection Strategies (ICLIPS) framework [van Minnen *et al.*, 2000; Füssel and van Minnen, 2001; Füssel *et al.*, 2003], with only a few studies covering the potential impact of climate change on water resources (e.g., the one by Fowler [1999] for New Zealand).

[26] In general, response surfaces (RS) express the response of a system to the variation of two or more driving variables. The RS is hereby derived by individual system simulations for each combined incremental change in the driving variables, representing a sensitivity analysis. The results of each model simulation form one discrete data

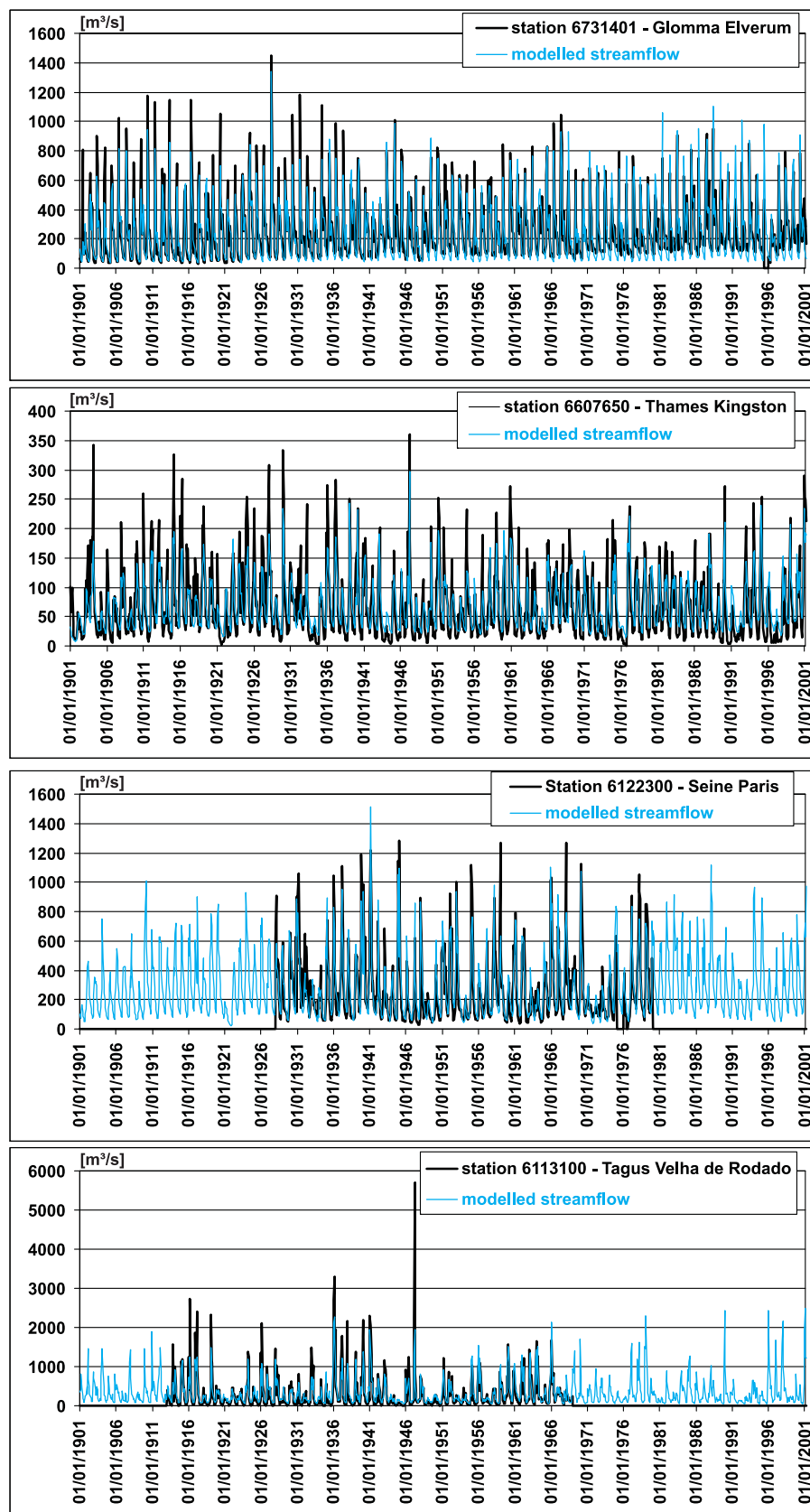


**Figure 1.** Time series of simulated versus observed streamflow for selected basins. Efficiency indices can be found in Table 1.

**Table 1.** Model Validation for Selected Catchments<sup>a</sup>

River	Station	Name	Measured				Simulated				$R^2$	Bias ( $m^3/s$ )	NSE
			Area ( $km^2$ )	Mean ( $m^3/s$ )	Maximum ( $m^3/s$ )	Volume ( $10^6 m^3$ )	Area ( $km^2$ )	Mean ( $m^3/s$ )	Maximum ( $m^3/s$ )	Volume ( $10^6 m^3$ )			
Glomma	6731401	Elverum	15,426	247.09	1,447.35	782.96	14,828	234.22	1,339.85	742.91	0.83	12.87	0.83
Thames	6607650	Kingston	9,948	67.48	359.47	216.10	10,202	67.51	297.28	216.38	0.72	-0.03	0.69
Seine	6122300	Paris	44,320	268.86	1,284.00	427.57	43,402	267.88	1,516.94	426.013	0.75	0.98	0.75
Tagus	6113100	Velha de Rodado	59,167	309.25	5,708.00	542.33	60,024	332.17	2,279.83	583.632	0.74	-22.92	0.72

<sup>a</sup> $R^2$  is from equation (1), bias is from equation (2), and NSE is from equation (3).

point in the 3-D response space and can then be interpolated to a continuous surface, the response surface.

[27] In this study, RS are used to assess the sensitivity of water availability to climate change. Temperature and precipitation are selected as the most important climate variables driving the hydrological cycle. The reference climate time series is perturbed at predefined increments of  $1^\circ\text{C}$  in the range  $[-1^\circ\text{C}, +6^\circ\text{C}]$  for temperature ( $T$ ) and at increments of 10% in the range  $[-40\%, +100\%]$  for precipitation ( $P$ ). This range was chosen to encompass the envelope of changes projected for Europe by the currently available regional climate models (see below) up to the year 2100 and beyond.

[28]  $T$  changes were added to the reference climate time series, and  $P$  changes were multiplied by the reference climate time series. For each combination of modified reference climate, a 30 year impact model run was carried out. The resulting time series of water availability were averaged to a 30 year average annual water availability of each basin and plotted as one value into a 3-D plot (see Figure 2a). The individual points were then interpolated to a continuous surface (Figure 2b).

[29] Since the sensitivity to an average annual change is examined, there exist two ways of perturbing the reference climate: First, the monthly climate is perturbed with a constant value. An example is given in Figure 3a for a perturbation of temperature of  $2^\circ\text{C}$ . In each month,  $2^\circ\text{C}$  are added to the reference climate (here shown for 12 months). However, it is well-known that climate change is not evenly distributed to the months of the year. A second possibility is hence to distribute the average annual change according to the seasonal cycle as given by climate model projections (Figure 3b), i.e., to calculate monthly scaling factors for the

distribution of annual climate change. For this study, the second possibility is chosen because it is considered to be more realistic.

[30] Modeling climate change is still subject to considerable uncertainty. Therefore, the average of the results of six different RCMs for 2071–2100 (Table 2) is used to distribute the average annual changes to the months of the year. Here the average annual change is broken down to varying monthly changes by calculating normalized monthly scaling factors from the difference of scenario climate data to the reference period data set. Thus, the projected future climate cycle is taken into account in each grid cell. For each of the six RCMs, a period of 30 years is used for both the reference period (1961–1990) and the scenario period (2071–2100) to construct mean monthly scaling factors.

[31] On the basis of the model internal disaggregation of monthly precipitation input to daily values, again, two approaches of adding delta changes are differentiated. On the one hand, increased precipitation values can be generated by increasing the intensity of precipitation while preserving the number of wet days per month at the 1961–1990 values. On the other hand, the number of wet days per month can be increased, while maintaining rainfall intensities at the 1961–1990 levels. Obviously, the second approach is confined by the number of days per month. Once all wet days in a month are assigned, the intensity of precipitation will increase. Both approaches are analyzed in this study.

## 2.6. Spatial-Temporal Aggregation and Selected River Basins

[32] The impact model works with a spatial grid cell resolution of  $0.5^\circ$  and is driven by climate data on that same resolution. Resulting water availability is examined at river

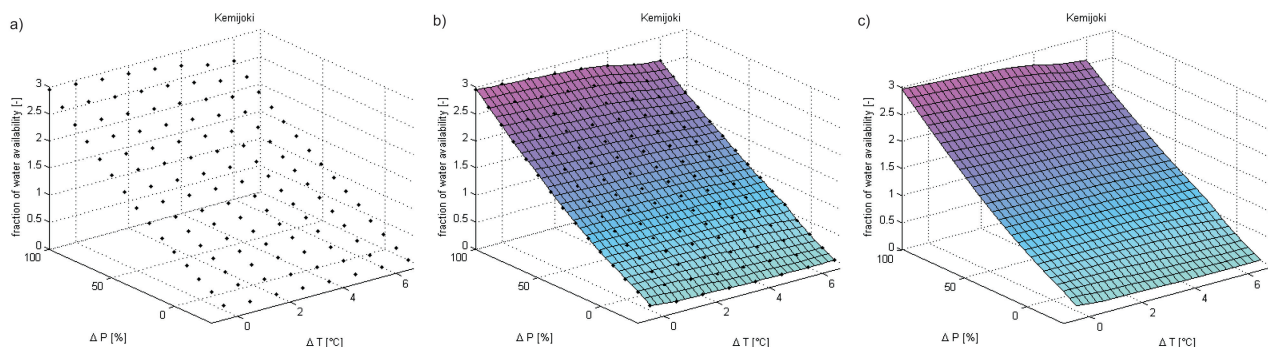


**Figure 2.** Construction of the response surfaces. (a) Long-term average annual water availability resulting from individual impact model simulations for perturbed reference climate. (b) The points interpolated to a continuous surface. (c) Response surface without underlying discrete simulation results.

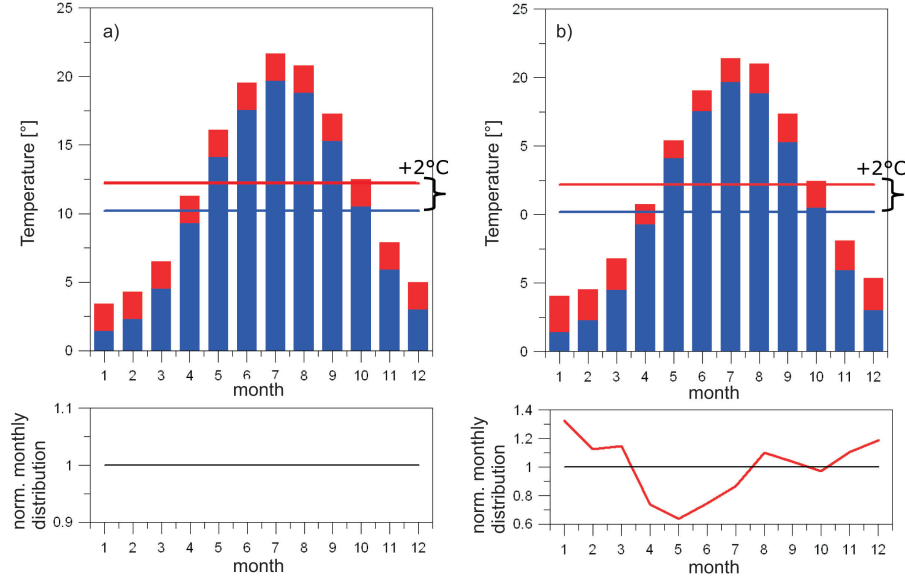


**Figure 3.** Two ways of distributing average annual temperature perturbation to the months: (a) equal perturbation in each month and (b) perturbation according to an average projected seasonal cycle.

basin scale. No specific years are analyzed; instead, 30 year periods are used. Current conditions are represented by the period 1961–1990; the year 2100 is represented by the period 2071–2100.

[33] The European climate varies from cold temperate, potentially subarctic, in the north to temperate with mild wet winters and hot, dry summers in the south. Water resources and precipitation are unevenly distributed: precipitation is highest in the western part and in mountain areas. Annual average runoff ranges from 3000 mm in western Norway to 100–400 mm over much of central Europe to less than 25 mm in southern Spain. We have selected 18 climate-representative river basins across Europe (Figure 4). Figure 5 shows current long-term annual precipitation and temperature averages in the selected river basins according to the 1961–1990 CRU TS 2.1 climate data set [Mitchell and Jones, 2005].

## 2.7. Sensitivity Assessment and Sensitivity Classification

[34] After constructing response surfaces for each of the 18 catchments (see section 2.5), the nature of the system itself is examined, i.e., the shape of the response surface and its position in the 3-D space. As the same increments for all catchments are used to generate response surfaces of normalized water availability, results can be directly compared. The first indicator analyzed is the volume below the surface, as shown in Figure 6. It is assumed that the greater the volume is, the more sensitive the system responding to climate change is.

[35] As a second indicator we examine the stability of the flow regime under climate change. The natural flow regime has been identified as critical to the ecological integrity of a system [Richter *et al.*, 1996; Poff *et al.*, 1997; Gibson *et al.*, 2005]. A delay in the occurrence of the peak month can, for example, severely affect freshwater biodiversity [Tockner and Stanford, 2002].

[36] The stability of the flow regime is assessed by analyzing the basin-specific Pardé coefficient curve [Pardé, 1933; Krasovskia *et al.*, 1994; Bower *et al.*, 2004]. It is constructed by normalizing the monthly flow by the long-term annual mean flow. For each combination of climate change parameters, Pardé coefficient curves are calculated as the average of a 30 year period to neglect short-term fluctuations in water availability. The stability of the flow regime under climate change is expressed as Pardé curve displacement. The Pardé curve displacement is calculated as the sum of the areas between the reference period curve and each of the “perturbed” curves (Figure 7). For the calculation of the area, unity width is assumed for each month.

[37] In order to rank the basins according to their sensitivity, the volume under the response surface is normalized by the mean volume of the 18 analyzed basins, revealing which basins react stronger than average (value >1.0) and which basins show a response weaker than average (value <1.0).

[38] Similarly, the displacement indicator is averaged by the mean displacement to facilitate intercomparison of basins. Both indicators are then equally weighted, and the basins are ranked according to the mean of both indicators.

**Table 2.** Regional Climate Models (RCMs) as Applied in This Study

RCM	Driving General Circulation Model	Scenario	Reference <sup>a</sup>
C4I-RCA3	HadCM3-e1	A1B	Ensembles Project
DMI-HIRHAM5	ARPEGE	A1B	Ensembles Project
ETHZ-CLM	HadCM3Q0	A1B	Böhm <i>et al.</i> [2006]
KNMI-RACMO2	ECHAM5	A1B	Ensembles Project
MPI-M-REMO	ECHAM5	A1B	Jacob [2001], Jacob <i>et al.</i> [2001]
SMHI-RCA3	BCM	A1B	Kjellström <i>et al.</i> [2005]

<sup>a</sup>For the Ensembles Project, see <http://ensembles-eu.metoffice.com/index.html>.

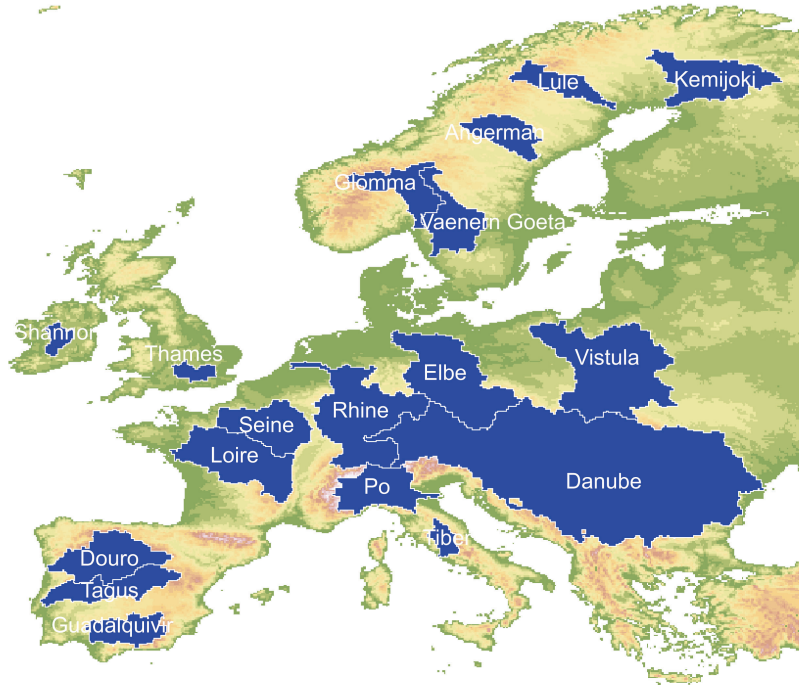


**Figure 4.** Selected European river basins.

## 2.8. Vulnerability Assessment

[39] While the sensitivity of a system is a measure of the pure response of a system to a certain trigger, the vulnerability includes information on the system's capacity to cope with the triggered conditions. In the first case, system refers to an analyzed unit, here a river basin. In the latter, the system encompasses individuals or communities within that system, which are impaired by the system's response, e.g., societies or plant communities within the boundaries of, for example, a river basin. Their necessity and ability to react to and cope with change is expressed in the vulner-

ability. Here RS created in section 2.7 are used to investigate whether societal thresholds are exceeded under climate change conditions to estimate the vulnerability of the human population within the analyzed river basins.

### 2.8.1. Thresholds

[40] Thresholds mark the critical state in a system, beyond which the proper functioning and integrity of the system might not be guaranteed. The response of a system to the exceedance of a threshold can either be linear or non-linear; that is, the system is pushed in gradual steps past a defined critical limit, or the incremental increase of the

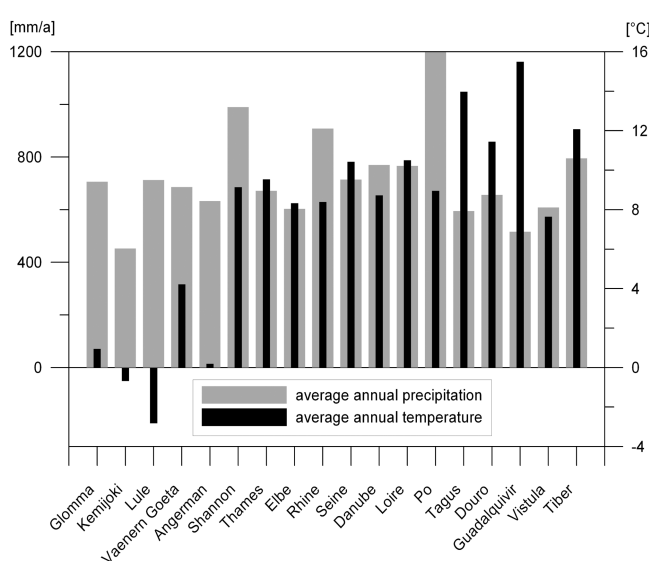


**Figure 5.** Long-term average annual precipitation and temperature of the selected river basins (1961–1990) based on CRU TS 2.1.

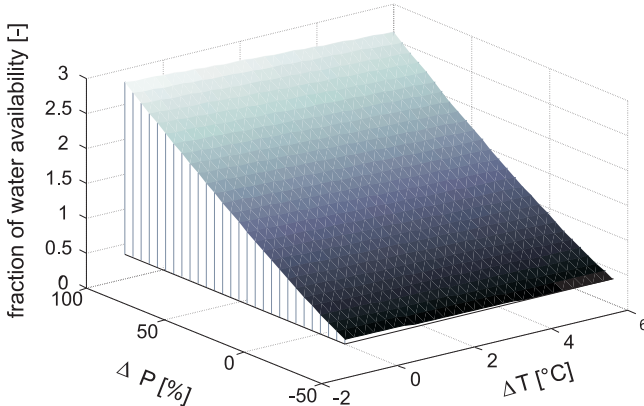


**Figure 6.** Volume below the response surface as a measure of a basin's response to climate change.

trigger causes an abrupt, disproportionate jump in response [Arnell, 2000; Groffman *et al.*, 2006]. The combination of the threshold analysis with response surfaces supports impact analysis in two ways: In a linear response system, predefined thresholds reveal unacceptable limits of change. In a nonlinear system, the response surface reveals a threshold and hence an unacceptable limit of change by a sudden bend in the surface.

[41] Thresholds from the categories of high flow, low flow [Smakhtin, 2001; Laaha and Blöschl, 2008], and water stress were chosen for this study [Postel, 1997; Falkenmark and Widstrand, 1992; Henrichs *et al.*, 2002; Alcamo *et al.*, 2003b; Flörke and Alcamo, 2007]. As low- and high-flow indicators the  $Q_{80}$  and  $Q_{20}$  flows are used [Clausen and Biggs, 2000; Olden and Poff, 2003; Monk *et al.*, 2007], representing the flow that statistically is exceeded 80% or 20% of the time, respectively, determined from flow duration curves.

[42] Water stress is examined using two indicators. The first indicator is the water availability index (WAI), defined as the amount of annual renewable fresh water per capita accessible to anthropogenic uses (excluding fossil groundwater), for which the following thresholds are commonly used. Below 1700 m<sup>3</sup> per capita and year, periodic high water stress is experienced. Below 1000 m<sup>3</sup> per capita and year, chronically high water stress is experienced, which could negatively influence economic development and human health. Below 500 m<sup>3</sup> per capita and year, absolute water scarcity is experienced [Falkenmark and Widstrand, 1992; Gleick, 1993; Postel, 1997; World Bank, 1992].

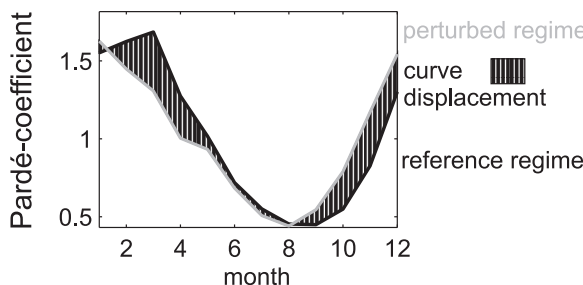


**Figure 7.** Calculation of the displacement of the flow regime curve caused by temperature and precipitation perturbations.

These values are converted to thresholds of water availability by multiplying with data on population per basin provided by the *Center for International Earth Science Information Network* [2005].

[43] As an alternative to the WAI (fresh water per capita), which overemphasizes densely populated areas, we further apply the indicator withdrawal-to-availability ratio (WTA), i.e., the sum of water withdrawn in the domestic, industrial, and agricultural sectors divided by the total annual renewable water resource of a basin. Categories of water stress are low for a WTA <0.2, medium for a WTA between 0.2 and 0.40, and severe for a WTA >0.4 [Alcamo *et al.*, 2007]. Again, we convert these values into thresholds of water availability by reversing this equation and solving for water availability at constant withdrawals. Withdrawals are as calculated with WaterGAP for current conditions. The normalized flow and water stress thresholds of each basin are plotted onto the response surfaces.

## 2.8.2. Vulnerability Classification

[44] For six different RCMs (Table 2), basin averages of  $T$  and  $P$  change under the IPCC A1B scenario for the year 2071–2100 are calculated. These are superimposed over the response surfaces. The vulnerability classification is carried out on the basis of the absolute number of climate projections under which the above described thresholds would be violated in the year 2100 (2071–2100).

[45] Table 3 gives the key to the vulnerability classification with the high- and low-flow indicators. The key to the vulnerability classification with the water stress indicators WAI and WTA is given in Table 4. Here the current state of the basin is of relevance to the vulnerability classification. For example, a basin that is currently not stressed will be classified with a plus if the low water stress threshold is violated according to any 1–6 RCM simulations. If the medium water stress threshold is violated by any 1–6 RCM simulations for that same basin, it will be classified with two pluses. As another example, we look at a basin that is currently classified as medium water stressed. If RCM simulations suggest that this medium water stress threshold is violated by 1–3 simulations in the future only, it is assumed that a relaxation of the water stress situation will take place, and the basin is classified as a plus. If it remains in its medium water stressed class (as projected by 4–6 RCM simulations). It will be rated with two pluses, and if it moves up into the next (high) water stress class, it will be rated with three pluses. See Table 4 for any other configurations of current and future water stress classes.

[46] For the vulnerability ranking, we chose from the two analyzed water stress indicators the one that resulted in the higher stress class. The water stress indicator and high-

**Table 3.** Key to Vulnerability Classification for the High- and Low-Flow Indicators<sup>a</sup>

Indicator	TVNS			
	0	1	2–3	4–6
High flow	0	+	++	+++
Low flow	0	+	++	+++

<sup>a</sup>The classification scheme is as follows: 0, not vulnerable; +, low vulnerability; ++, medium vulnerability; +++, high vulnerability. TVNS, threshold violated by number of scenarios.

**Table 4.** Key to Vulnerability Classification for the Water Stress Indicators<sup>a</sup>

Current	Future						
	No TVNS	Low 1–3	Low 4–6	Medium 1–3	Medium 4–6	High 1–3	High 4–6
None	0	+	+	++	++	+++	+++
Low	0	0	+	++	++	+++	+++
Medium	0	0	0	+	++	+++	+++
High	0	0	0	+	++	++	+++

<sup>a</sup>See Table 3 for description of symbols. TVNS, threshold violated by number of scenarios.

and low-flow indicators were then equally weighted on the basis of the sum of plus signs, and again, the basins were compared to each other, ranking them from highest to lowest vulnerability.

### 3. Results

#### 3.1. Sensitivity Analysis Results

[47] In section 2 we introduced two alternative approaches to apply delta changes to precipitation, which were (1) increasing the rainfall intensity at constant number of wet days and (2) increasing the number of wet days and thus maintaining the rainfall intensity. The results of both alternatives will now be shown for a basin in a cool climate (Kemijoki) and one in a warm climate (Guadalquivir). In Figures 8 and 9, contour plots show the response of water availability to climate change based on both approaches for the Kemijoki and Guadalquivir basins.

[48] For both approaches we find an overproportional increase in water availability compared to the initial perturbation in precipitation at the Kemijoki basin and for the Guadalquivir under approach 1. For approach 2, the same pattern became more pronounced for larger changes in pre-

cipitation, while for small delta changes, water availability responded proportionally less.

[49] This result occurs because the additional water is partitioned differently between the various moisture storages. Table 5 shows the water balance for both basins and both approaches of disaggregating delta changes for a parameter perturbation of  $\Delta T = +6^\circ\text{C}$  and  $\Delta P = +100\%$ . Table 5 confirms that the mass balance with respect to volume of water is also preserved for extreme perturbations. Adding rainfall on an already wet day tends to exceed soil water capacity, converting the additional water almost entirely into direct runoff. In the results below, we will therefore use the assumption that additional rain will be distributed to additional wet days, thus maintaining intensity at reference level until the maximum number of days per month is reached. The response of water availability in this approach is less disproportionate.

[50] Figure 10 shows response surfaces for the 18 analyzed European catchments, representing the sensitivity of annual water availability to changes in temperature and precipitation. To enable a comparison between basins, water availability is normalized by its reference value (1961–1990). Figure 10 indicates that the response of the selected basins is quite similar, differing mainly in magnitude; water

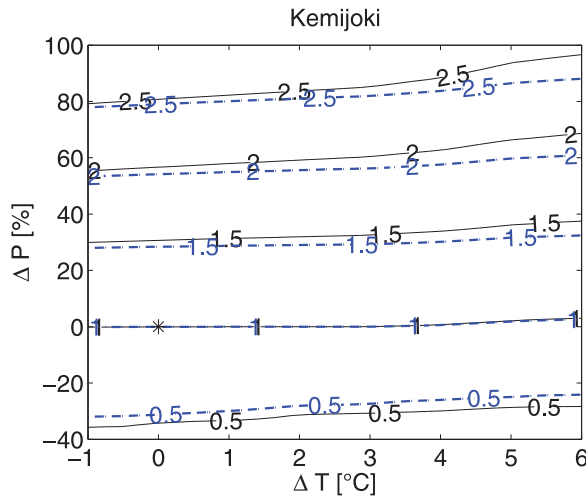


**Figure 8.** Contour plots of annual water availability for the Kemijoki basin as fractions of current mean annual water availability based on two approaches of applying precipitation delta changes. Blue dashed lines show increasing rainfall intensity at a constant number of wet days, and black solid lines show increasing the number of wet days while maintaining rainfall intensity. The x and y axes show average annual changes in  $T$  and  $P$ .

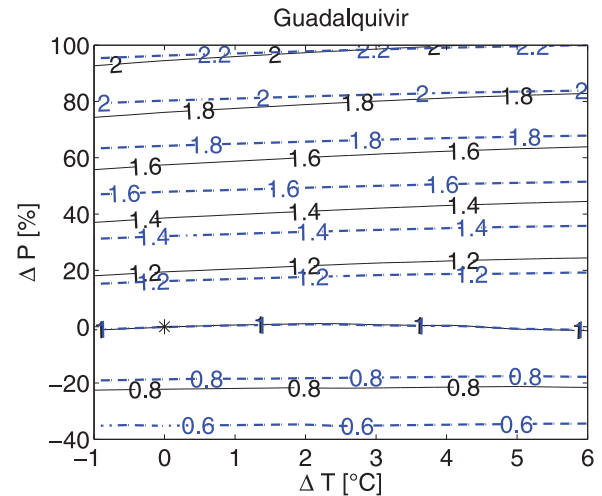


**Figure 9.** Contour plots of annual water availability for the Guadalquivir basin as fractions of current mean annual water availability based on two approaches of applying precipitation delta changes. Blue dashed lines show increasing rainfall intensity at constant number of wet days, and black solid lines show increasing the number of wet days while maintaining rainfall intensity. The x and y axes show average annual changes in  $T$  and  $P$ .

**Table 5.** Water Balance Components for Parameter Perturbations of  $\Delta T = +6^{\circ}\text{C}$  and  $\Delta P = +100\%$  for the Kemijoki and Guadalquivir, With Delta Changes of Precipitation Added Either by Increasing the Number of Wet Days (NRD) or by Increasing Intensity at Constant Number of Wet Days (Intensity).<sup>a</sup>

River Basin	Delta Change	Precipitation ( $\text{km}^3$ )	AET ( $\text{km}^3$ )	Surface Plus Groundwater Runoff ( $\text{km}^3$ )	Deviation in Water Balance ( $\text{km}^3$ )
Kemijoki	NRD	32.9	4.7	28.4	-0.20
Kemijoki	intensity	32.9	2.9	30.1	-0.18
Guadalquivir	NRD	76.4	15.9	60.7	-0.18
Guadalquivir	intensity	76.0	9.7	65.9	-0.10

<sup>a</sup>Precipitation, actual evapotranspiration (AET, including interception), and surface plus groundwater runoff are given as 30 year sums, averaged over all grid cells of a basin. Change in storage is assumed to be close to zero for a period of 30 years and is therefore not stated.

availability increases linearly with precipitation and decreases linearly or exponentially with temperature. The reason for the similarity is that the annual response curves average out opposing tendencies observed in monthly (and presumably smaller time scale) flows. Further on we show much stronger responses of the monthly time scale.

[51] Two metrics to compare response curves are used, i.e., the “volume below surface” (abbreviated “volume”), which indicates the response of annual water availability, and the “displacement of Pardé curves” (abbreviated “displacement”), which reflects the response of the monthly flow regime. See Figures 6 and 7 for an explanation of these metrics.

[52] As an example for the displacement of Pardé curves under changing climate, Figure 11 gives three sample plots of Lule, Danube, and Tiber for an increase in temperature by  $3^{\circ}\text{C}$ . The change in precipitation between  $-40\%$  and  $+100\%$  is depicted with colored curves ranging from blue to green. The 1961–1990 reference curve is shown as black. More examples of Pardé curves for different temperature variations are given in the auxiliary material.<sup>1</sup>

[53] The stability of the flow regime depends mainly on the three following aspects: (1) Is the basin situated in a snow climate, and does temperature change therefore effect the timing of snowmelt? (2) Is evapotranspiration energy limited or water limited; that is, does an increase in precipitation result in an increase in evapotranspiration or an increase in runoff? (3) How similar are current and future precipitation (and temperature) cycles; that is, is the discharge hydrograph shift in time due to a shift in precipitation (and temperature) timing?

[54] In the Lule basin, aspect 1 leads to a shift of the peak discharge to an earlier date and a slight flattening of the discharge hydrograph with increasing temperature. The Danube basin is heavily influenced by a shift in the future precipitation (and temperature) cycle, which leads to flattening of the discharge hydrograph throughout the year. In the Tiber basin, hardly any shift in Pardé curves becomes visible, which can be attributed to the water limitation of evapotranspiration and a similar current and future precipitation (and temperature) cycle.

[55] Both volume and displacement have been normalized by their average in order to compare the analyzed basins among one another. Figures 12 and 13 show that the normalized volume ranges from 0.7 (Guadalquivir) to

1.24 (Loire), while the normalized displacement ranges from 0.3 (Guadalquivir) to 2.1 (Lule). Apparently, there is a much wider range of responses of the monthly flow regimes than of annual water availability. Figures 12 and 13 also show that the monthly flow regimes of some basins might have a strong response to climate change while their annual water availability has a weak response (e.g., Lule) or the other way around (e.g., Elbe). In Figure 14, volume and displacement indicators are plotted against each other. A classification of the basins according to their location in northern, central, and southern European basins is also shown.

[56] If equal weight is given to the sensitivity of annual water availability and monthly flow regime, the sensitivity ranking of the basins in Table 6 is obtained. The first four are northern basins heavily influenced by snowpack and snowmelt. The last two are the Douro and Guadalquivir, located in the semihumid areas of the Iberian Peninsula. Falling in the middle of the ranking are the Loire and Rhine.

[57] To understand their sensitivities, it is helpful to examine the response surfaces of monthly flows shown for three selected basins: the Angerman for northern Europe, the Elbe for central Europe, and the Douro for southern Europe. Figure 15 shows four specific months for each of these three basins. More plots of normalized monthly water availability are given in the auxiliary material.

[58] The Angerman basin, strongly affected by snowmelt, shows significantly different forms of response for different months. Monthly responses are much more pronounced than the curves for annual water availability. In June, water availability declines exponentially as temperatures become warmer because the snowmelt, which currently feeds June discharge, is then shifted to earlier in the year. It is apparent that much of the snowmelt and resulting high river flows are shifted to April, which shows a very sharp peak in water availability as precipitation and temperature increase. A similar but milder effect is observed in the curve for March.

[59] Snowmelt only has a small affect on the Elbe hydrograph, which is by far not as pronounced as in the northern European basins because of the moderate climate along most of its length. The high-flow effect, which is present in the Angerman basin because of snowmelt, is also present, although in an earlier month and because of a combination of altered snowmelt and precipitation (and temperature) cycles. While the discharge declines in June in Angerman, it diminishes much earlier in the Elbe basin. This is apparent from the April response curve of the Elbe basin, which bears a distinct resemblance to the June curve of Angerman. As for the Angerman curve for April, the Elbe curves for December, January, and February show sharply increasing

<sup>1</sup>Auxiliary materials are available in the HTML. doi:10.1029/2009WR008516.

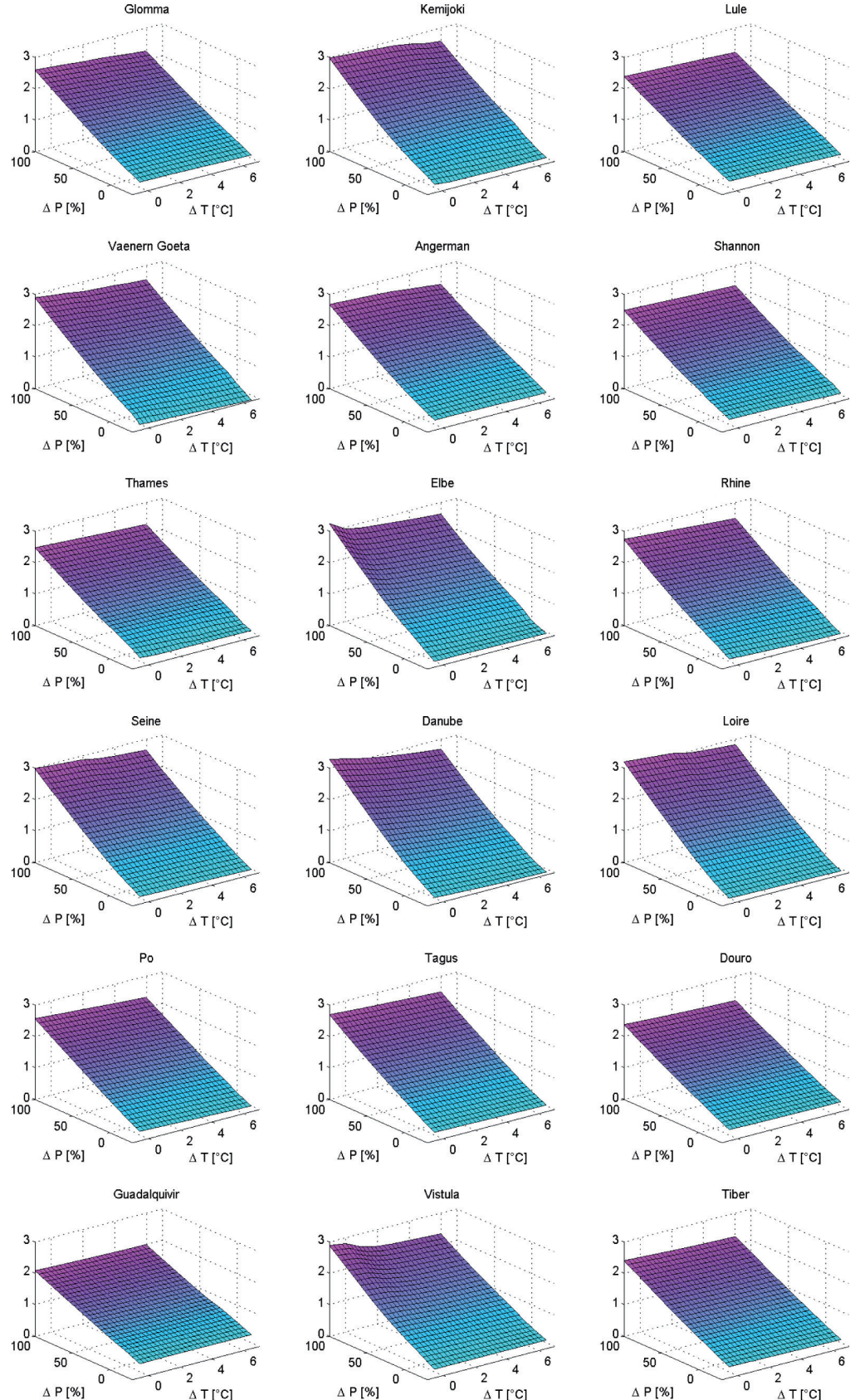


**Figure 10.** Response surfaces of the fraction of annual water availability resulting from temperature and precipitation perturbations. The  $x$  and  $y$  axes show annual changes in  $P$  and  $T$ , and the  $z$  axis gives the water availability normalized by its 1961–1990 value.

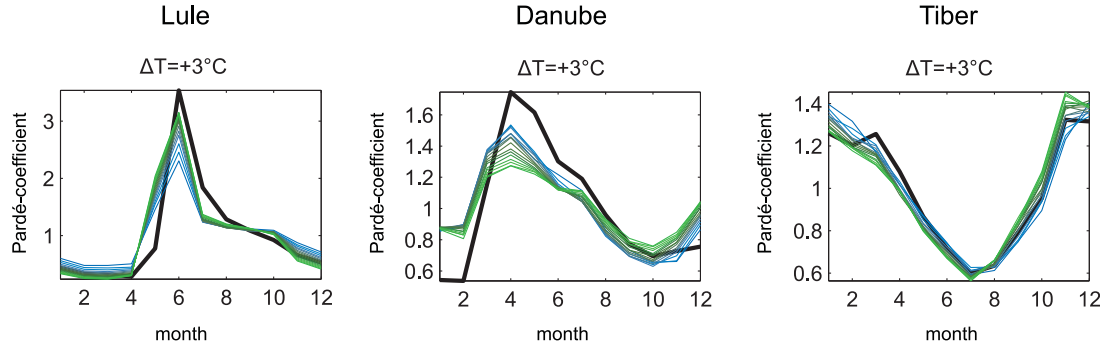


**Figure 11.** Pardé coefficient curves for the Lule, Danube, and Tiber rivers for a perturbation of temperature of  $+3^{\circ}\text{C}$ . The black curve is the 1961–1990 reference curve, and the colored curves are the curves resulting from a variation of  $P$  between  $-40\%$  and  $+100\%$  (blue to green).

water availability with increasing precipitation and temperature. However, water availability in the Elbe does not peak as sharply as in Angerman because when temperature increases above roughly  $2^{\circ}$  in the Elbe basin, increased evapotranspiration compensates for the increase in precipitation and slows the rise of water availability.

[60] The Douro shows a smaller response than the basins of northern and central Europe chiefly because warmer, sunnier conditions here promote the evaporation of a larger fraction of additional precipitation. The future precipitation cycle is similar to current conditions and does not alter the course of the discharge hydrograph. Similar to the Tiber, the main discharge takes place in the winter months with little streamflow in the summer months (also see Figure

11). Observed responses to climate change in the different months is therefore similar.

### 3.2. Vulnerability Analysis Results

[61] Although the 3-D response surfaces are visually interesting, they are difficult to interpret numerically. Therefore, we represent the same data as shown in Figure 10 in 2-D contour plots (Figure 16). Further, we superimpose the positioning of six climate scenarios, as explained in section 2.8, for the period 2071–2100 onto the temperature and precipitation space. This gives us a general method for looking at the implications of any particular climate scenario at any juncture in the future, as long as it fits on

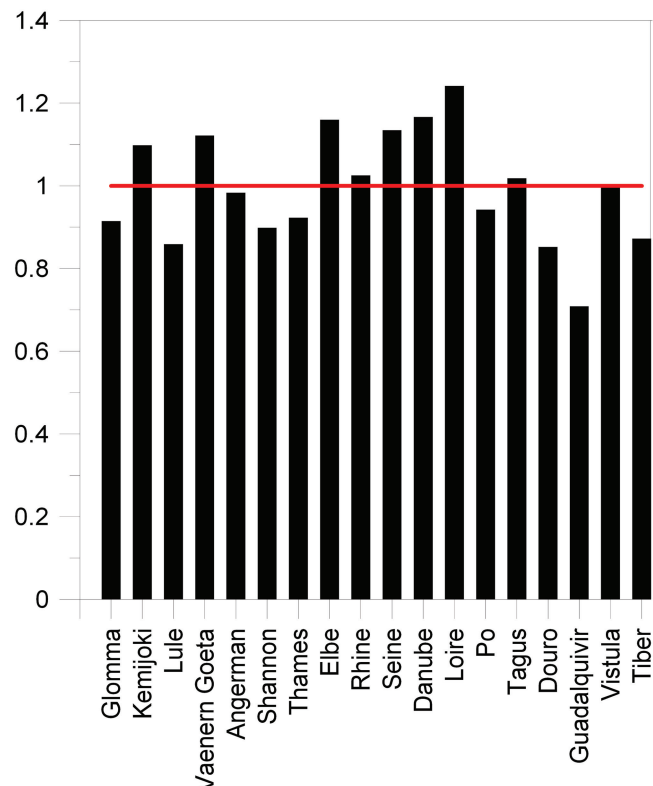


**Figure 12.** Volume below the response surface for the analyzed basins in relation to each other.

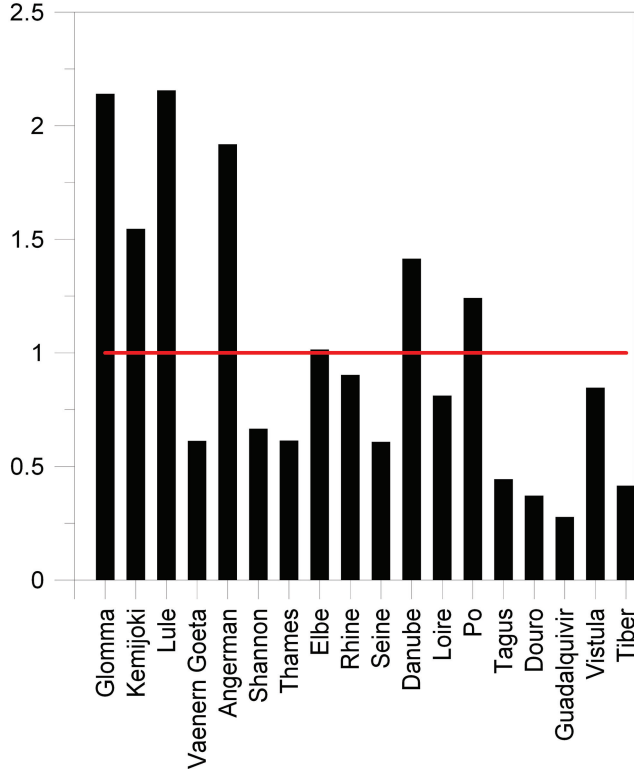


**Figure 13.** Displacement of the flow regime curves for the analyzed basins in relation to each other.

the given temperature and precipitation domain. With this diagram we combine an estimate of the future pressure on water resources (the climate changes represented by the climate scenarios) with the sensitivities of the river basins (as represented by the response surface diagrams) in order to

assess the vulnerability of the river basins to climate change by indicating various thresholds for extreme flows and water stress relevant to the populations living in these basins. Obviously, the vulnerability classification presented here is subjective to the chosen thresholds.

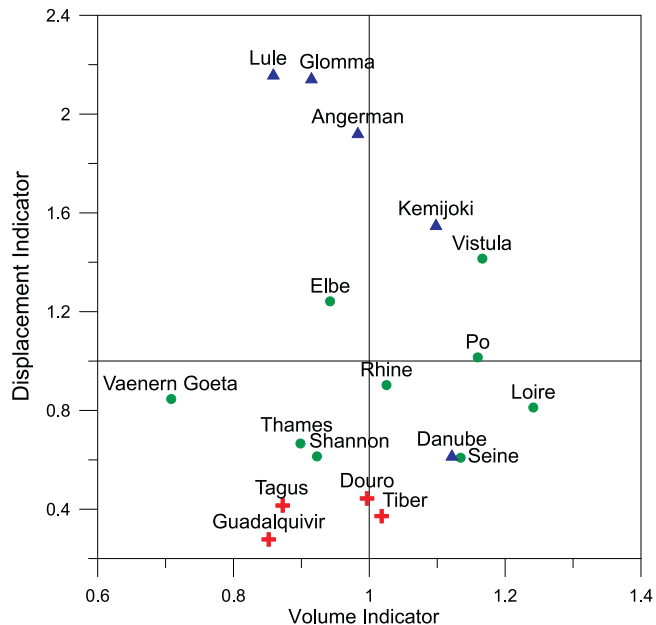


**Figure 14.** Sensitivity indicators plotted against each other, with a geographical classification of basins into northern (blue triangles), central (green circles), and southern (red crosses) Europe.

**Table 6.** Sensitivity Ranking of 18 European Basins Based on Two Indicators of System Behavior, Volume and Displacement

River Basin	Volume	Displacement	Average
Glomma	0.91	2.14	1.5
Lule	0.86	2.16	1.5
Angerman	0.98	1.92	1.5
Kemijoki	1.10	1.55	1.3
Danube	1.17	1.41	1.3
Po	0.94	1.24	1.1
Elbe	1.16	1.01	1.1
Loire	1.24	0.81	1.0
Rhine	1.03	0.90	1.0
Vistula	1.00	0.85	0.9
Seine	1.13	0.61	0.9
Vaenern Goeta	1.12	0.61	0.9
Shannon	0.90	0.67	0.8
Thames	0.92	0.61	0.8
Tagus	1.02	0.44	0.7
Tiber	0.87	0.41	0.6
Douro	0.85	0.37	0.6
Guadalquivir	0.71	0.28	0.5

[62] As described earlier we define different vulnerability classes for the river basins according to the number of climate scenarios violating different thresholds. (See Tables 3

and 4 for the definition of these vulnerability classes.) The resulting vulnerability ranking (Table 7) is quite different from the sensitivity ranking (Table 6). The relatively insensitive southern river basins, such as Douro and Guadalquivir, are much higher in the vulnerability ranking because expected changes in precipitation and temperature according to the climate scenarios lead to higher water stresses. Other river basins, such as the Vistula, that have a medium sensitivity ranking are at the top of the vulnerability list because of the combination of moderate sensitivity and unfavorable climate changes according to the scenarios. On the other hand, the Shannon, which has a moderate sensitivity ranking, has the lowest vulnerability because the given climate scenarios do not lead to large unfavorable changes in water availability.

[63] The span of projected percentage changes in water availability based on the different scenario calculations is shown as box-whisker plots in Figure 17 for all 18 river basins. These are derived from the response surfaces by computing water availability at the intersection of the  $T$  and  $P$  change as given by the different RCMs. The lengths of the whiskers represent the spread in water availability caused by the different RCM projections in each basin. Overall, we find a gradient in changes that starts in northern

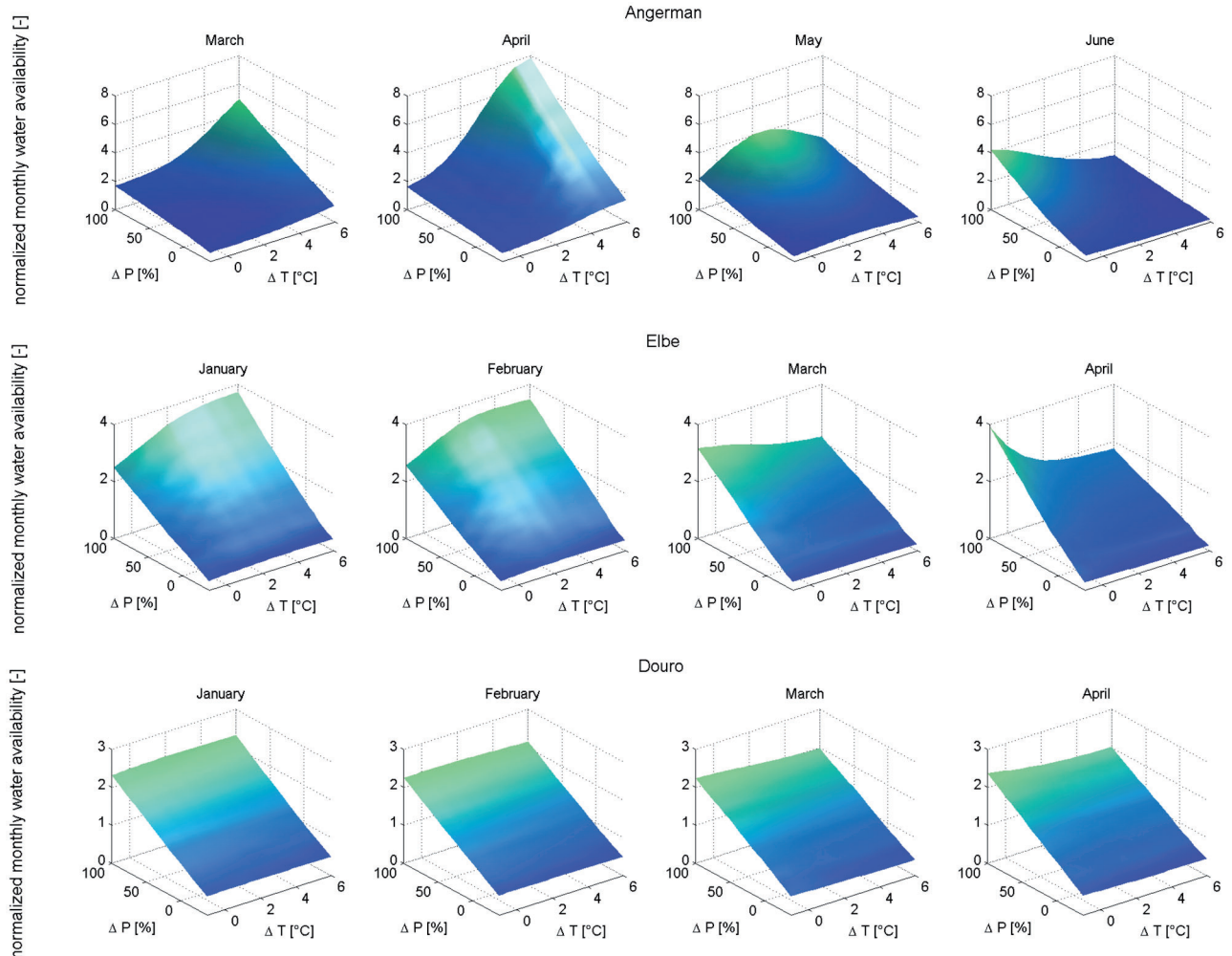


**Figure 15.** Response surfaces of normalized monthly water availability for specific months for Angerman, Elbe, and Douro.

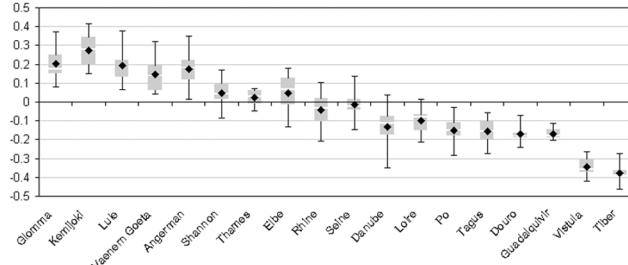


**Figure 16.** Contour plots of annual water availability including societal thresholds of tolerance and the positioning of six climate change projections for 18 European catchments.

Europe with increasing water availabilities and ends in southern Europe with a decrease in water availability. The strongest decrease in water availability is observed for the Vistula and Tiber basins. Central Europe is the transition area between the increase in the north and the decrease in the south. Results for those basins are therefore inconclusive, and the direction of change depends strongly on the respective RCM.

#### 4. Discussion and Conclusions

[64] Using the response surface method enabled us to consistently and objectively compare the sensitivity of European river basins to climate change and carry out a vulnerability assessment based on the results of six RCMs for the IPCC A1B emissions scenario, subjected to the chosen societal windows of tolerance for water availability levels. All basins were analyzed on the basis of the same rules, indicators, and thresholds.

[65] The most sensitive to climate change were the Nordic basins, e.g., Lule, Glomma, and Angerman, followed by central European basins, while southern European basins, e.g., Tagus, Douro, and Guadalquivir, were the least sensitive. Overall, the sensitivity of a basin depends on the following three aspects (or their combination): the number of days below freezing, the degree of water limitation of evapotranspiration, and the degree of change in the timing and magnitude of future temperature and precipitation.

[66] The high sensitivity of the Nordic basins can be explained by the fact that they are characterized by a mostly snow-dominated regime. Temperature increases directly affect the onset of high discharges because of snowmelt and therefore affect the stability of the flow regime. Of the Nordic basins, the Vaenern Goeta exhibits a comparably low sensitivity because of the large lake downstream, which dampens the effect on streamflow. In all other Nordic basins analyzed in this study, lakes and wetlands are situated upstream and therefore have a lower buffering effect. Central European basins are still medium in sensitivity because the distribution of the future precipitation and temperature might differ from the current situation and hence affect future flow regimes. Southern European basins are found to be the least sensitive under the chosen

**Table 7.** Vulnerability Ranking of 18 European Basins Based on the Equal Weighting of Two Indicators, High/Low Flow and Water Stress<sup>a</sup>

River Basin	High/Low Flow	Water Stress		Sum
		WAI	WTA	
Vistula	+++	++	+++	6
Tiber	+++	+	+++	6
Danube	+	0	+++	4
Kemijoki	+++	0	0	3
Thames	0	++	+++	3
Seine	0	0	+++	3
Tagus	0	0	+++	3
Douro	0	0	+++	3
Guadalquivir	0	+	+++	3
Angerman	+++	0	0	3
Lule	++	0	0	2
Rhine	0	+	++	2
Elbe	0	+	++	2
Vaenern Goeta	++	0	0	2
Glomma	++	0	0	2
Loire	0	0	++	2
Po	0	0	++	2
Shannon	0	0	0	0

<sup>a</sup>See Table 3 for description of symbols. WAI, water availability index; WTA, withdrawal-to-availability ratio.

indicators because evapotranspiration makes up a major component of the water balance and increasing precipitation can be counterbalanced by increasing evaporation, especially under rising temperatures.

[67] Our ranking of basins does not contradict previous studies, e.g., for Greece [Mimikou *et al.*, 1991, 2000], Spain [Avila *et al.*, 1996], the Rhine [Kwadijk and Rotmans, 1995; Middelkoop *et al.*, 2001], the United Kingdom [Mansell, 1997; Arnell, 1998; Limbrick *et al.*, 2000], and Scandinavia [Bergström *et al.*, 2001]. Because of the difference in selected indicators, impact models, baseline periods, and scenarios, a European-wide comparison, however, was difficult for the majority of these regional assessments until now.

[68] The vulnerability ranking is quite different from the sensitivity ranking and shows the southern European basins having much higher rankings on the basis of the higher

**Figure 17.** Projected fractional change in water availability as calculated with the WaterGAP model. Box whisker plots show the direction of change in long-term average water availability between current conditions (1961–1990) and 2100 (2070–2099). Whiskers give the span of changes that result from the use of six RCMs. The black diamond indicates the mean, the boxes show the second and third quartiles, and the space in between represents the median.

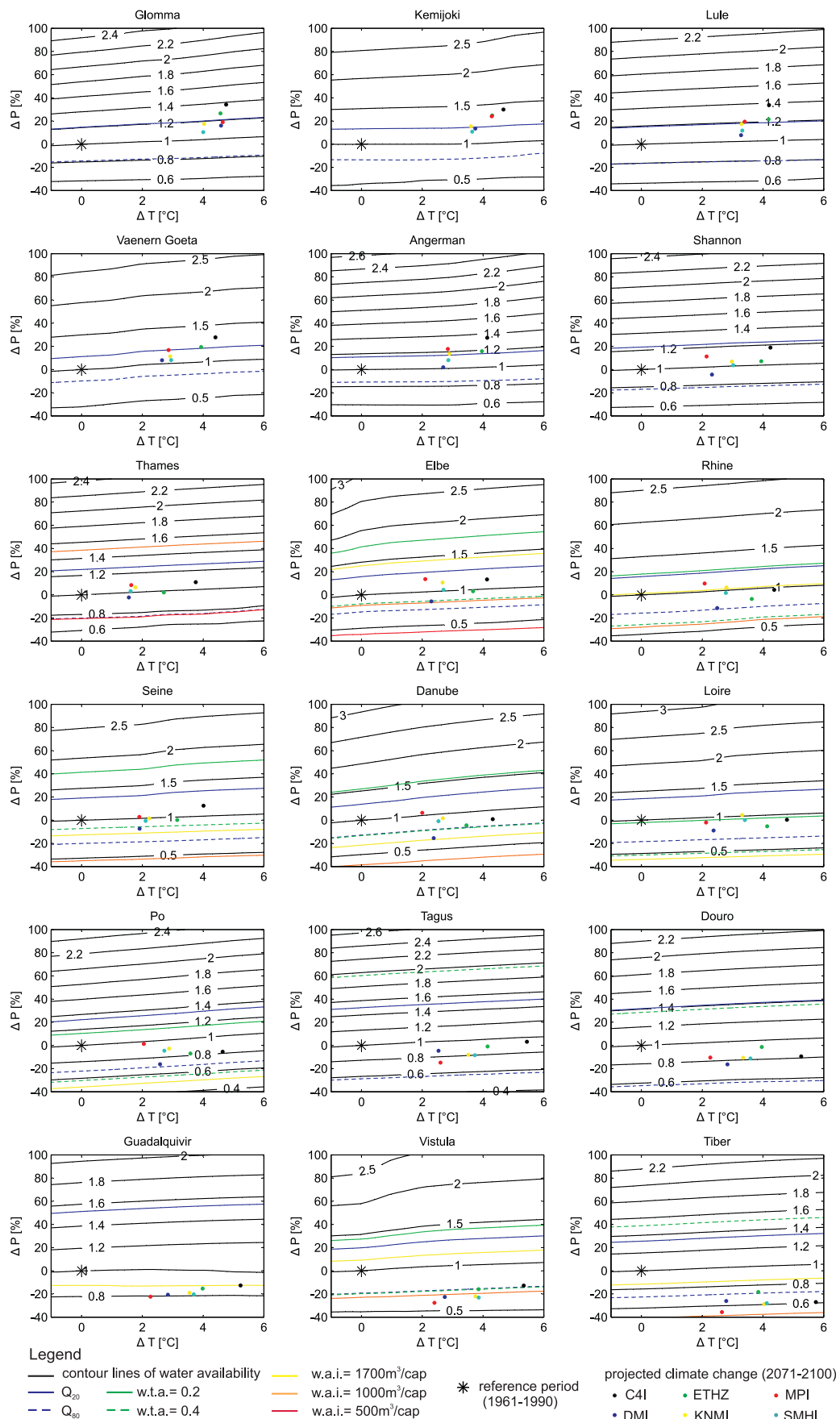


Figure 17

water stress levels they might face in the future. According to the indicators used here, the most vulnerable basins in Europe are the Vistula, Tiber, and Danube basins because both the high- and low-flow thresholds and water stress thresholds are violated under all of the six analyzed climate projections.

[69] The sensitivity of sectors under the influence of human management is closely associated with the development level, institutional capacities, and technological capabilities of society and can therefore be adapted within certain boundaries. The applied thresholds have been chosen on the basis of current knowledge and do not consider the adaptive capacity of society, possible changes in population densities, or the use of fossil groundwater to satisfy anthropogenic water needs. Thresholds might be subject to change, for example, because of improving technologies or different economical conditions, which could shift the sensitivity of a basin to a lower level. The use of different thresholds could therefore lead to a different vulnerability classification than the one found here. Also, only natural flow regimes were analyzed in this study. Some of the basins are already flow regulated under current conditions (e.g., the Glomma), and an adaptation of the flow regulation to the future situation could counteract some of the effects.

[70] On the other hand, the interpolation of an average intra-annual cycle from six different RCMs for the distribution of the climate change signal has leveled out extreme monthly changes and therefore might have led to a smaller response in some of the basins than with individual impact model simulations for each RCM. The use of different RCM projections for the same emissions scenario addresses only some uncertainties associated with projections of climate change, and it is quite possible that future climate change might put another area of the response surface into focus. However, because of the flexibility of the response surface method, new indicators or additional climate change frequencies could easily be included once they become available.

[71] Analyzing only one emissions scenario, we already find quite a spread in the response of water availability based on the projections of the six different RCMs. Although a logical result, its practical application, especially in the central European basins because of opposite tendencies, might be limited, for example, when planning adaptation strategies. This constitutes, however, a general problem when dealing with scenario studies. Further studies could seek to reduce this uncertainty, e.g., by increasing the number of climate models or the number of applied scenarios or with regard to the impact model used.

[72] Uncertainty arises from the fact only one global hydrological model was used to generate response surfaces. Although it was not possible to detect any correlation between the runoff correction factor or the runoff coefficient and the sensitivity by testing the Pearson product moment coefficient correlation, results most certainly depend on the physical representation of rainfall-runoff processes in the model applied here. Known uncertainties result, for example, from an overestimation of runoff in dry areas, as reported by a number of global hydrological models [Fekete *et al.*, 1999; Nijssen *et al.*, 2001], most likely due to neglecting evaporative transmission losses along the river channel. However, since a low sensitivity was found

for these basins, this error should have a rather small effect. Nonetheless, a continuation of this study could incorporate a greater number of hydrological models for the generation of response surfaces.

[73] The response surface method itself introduces some uncertainty caused by the fitting method, especially when extracting absolute values of projected water availability. The increased accuracy of the response surface with an increased number of generated points obviously collides with the desire to reduce the number of model runs and simulation time. Because of the rather linear behavior of water availability, this error seems negligible.

[74] Besides using thresholds adapted to socioeconomic scenario conditions or incorporating a greater number of hydrological models, future applications of the response surface method could investigate different parameters when testing the sensitivity of water availability to climate and global change, for example, a change in net radiation or the loss of natural biomes.

[75] On the whole, this procedure offers a consistent way to judge current and future conditions. It provides an immediate visual comparison of the relative impact of unit changes in the chosen parameters and enables the direct identification of hot spots, which might require further, detailed analysis.

[76] **Acknowledgments.** This study was carried out as part of the Ensembles Project (contract GOCE-CT-2003-505539), supported by the European Commission under the sixth Framework Program 2002–2006. The authors wish to thank the reviewers for their valuable comments.

## References

- Adam, J. C., E. A. Clark, D. P. Lettenmaier, and E. F. Wood (2006), Correction of global precipitation products for orographic effects, *J. Clim.*, **19**, 15–38, doi:10.1175/JCLI3604.1.
- Alcamo, J. M., P. Döll, T. Henrichs, F. Kaspar, B. Lehner, T. Rösch, and S. Siebert (2003a), Development and testing of the WaterGAP 2 global model of water use and availability, *Hydrol. Sci.*, **48**, 317–337, doi:10.1623/hysj.48.3.317.45290.
- Alcamo, J. M., P. Döll, T. Henrichs, F. Kaspar, B. Lehner, T. Rösch, and S. Siebert (2003b), Global estimates of water withdrawals and availability under current and future “business-as-usual” conditions, *Hydrol. Sci.*, **48**, 339–348, doi:10.1623/hysj.48.3.339.45278.
- Alcamo, J. M., D. van Vuuren, C. Ringler, W. Cramer, T. Masui, J. Alder, and K. Schulze (2005), Changes in nature’s balance sheet: Model-based estimates of future worldwide ecosystem services, *Ecol. Soc.*, **10**(2), 19 (available at <http://www.ecologyandsociety.org/vol10/iss2/art19/>).
- Alcamo, J. M., M. Flörke, and M. Märker (2007), Future long-term changes in global water resources driven by socio-economic and climatic changes, *Hydrol. Sci. J.*, **52**, 247–275, doi:10.1623/hysj.52.2.247.
- Arnell, N. W. (1998), Climate change and water resources in Britain, *Clim. Change*, **39**, 83–110.
- Arnell, N. W. (2000), Thresholds and response to climate change forcing: The water sector, *Clim. Change*, **46**, 305–316.
- Arnell, N. W., and C. Liu (2001), Hydrology and water resources, in *Climate Change 2001, Impacts, Adaptation, and Vulnerability. Contribution of Working Group II to the Third Assessment Report of the Intergovernmental Panel on Climate Change*, pp. 191–233, Cambridge Univ. Press, Cambridge, U.K.
- Avila, A., C. Neal, and J. Terradas (1996), Climate change implications for streamflow and streamwater chemistry in a Mediterranean catchment, *J. Hydrol.*, **177**, 99–116, doi:10.1016/0022-1694(95)02789-0.
- Bergström, S. (1995), The HBV model, in *Computer Models of Watershed Hydrology*, edited by V. P. Singh, pp. 443–476, Water Resour. Publ., Highlands Ranch, Colo.
- Bergström, S., B. Carlsson, M. Gardelin, G. Lindstrom, A. Pettersson, and M. Rummukainen (2001), Climate change impacts on runoff in Sweden: Assessments by global climate models, dynamical downscaling and hydrological modelling, *Clim. Res.*, **16**, 101–112.

- Böhm, U., M. Kücken, W. Ahrens, A. Block, D. Hauffe, K. Keuler, B. Rockel, and A. Will (2006), Clm—The climate version of lm: Brief description and long-term applications, *COSMO Newslett.*, 6, pp. 225–235, Dtsch. Wetterdienst, Offenbach am Main, Germany.
- Bower, D., D. M. Hannah, and G. R. McGregor (2004), Techniques for assessing the climatic sensitivity of river flow regimes, *Hydrolog. Processes*, 18, 2515–2543, doi:10.1002/hyp.1479.
- Box, G. E. P., and N. R. Draper (1959), A basis for the selection of a response surface design, *J. Am. Stat. Assoc.*, 54, 622–654.
- Box, G. E. P., and K. B. Wilson (1951), On the experimental attainment of optimum conditions (with discussion), *J. R. Stat. Soc., Ser. B*, 13, 1–45.
- Bruckner, T., G. Petschelt-Held, F. L. Tóth, H. M. Füssel, C. Helm, M. Leimbach, and H. J. Schellnhuber (1999), Climate change decision-support and the tolerable windows approach, *Environ. Model. Assess.*, 4, 217–234, doi:10.1023/A:1019076603956.
- Carpenter, S., P. Pingali, E. Bennett, and M. Zurek (Eds.) (2005), *Scenarios of the Millennium Ecosystem Assessment*, Island Press, Oxford, U.K.
- Center for International Earth Science Information Network (2005), Gridded Population of the World Version 3 (GPWv3): Population grids, Columbia Univ., Palisades, N. Y.
- Clausen, B., and B. J. F. Biggs (2000), Flow variables for ecological studies in temperate streams: Groupings based on covariance, *J. Hydrol.*, 237, 184–197, doi:10.1016/S0022-1694(00)00306-1.
- Collins, M. (2007), Ensembles and probabilities: A new era in the prediction of climate change, *Philos. Trans. R. Soc. A*, 365, 1957–1970, doi:10.1098/rsta.2007.2068.
- Cornell, J. A. (1987), *Response Surfaces: Designs and Analyses*, Marcel Dekker, New York.
- Döll, P., and B. Lehner (2002), Validation of a new global 30-min drainage direction map, *J. Hydrol.*, 258, 214–231, doi:10.1016/S0022-1694(01)00565-0.
- Döll, P., F. Kaspar, and B. Lehner (2003), A global hydrological model for deriving water availability indicators: Model tuning and validation, *J. Hydrol.*, 270, 105–134, doi:10.1016/S0022-1694(02)00283-4.
- Falkenmark, M., and C. Widstrand (1992), Population and water resources: A delicate balance, *Popul. Bull.*, 47, 2–35.
- FAO (2007), *Gridded livestock of the world 2007*, by G. R. W. Wint and T. P. Robinson, 131 pp., Rome.
- Fekete, B., C. J. Vörösmarty, and W. Grabs (Eds.) (1999), *Global Composite Runoff Fields of Observed River Discharge and Simulated Water Balances*, Global Runoff Data Cent., Koblenz, Germany.
- Fekete, B. M., C. J. Vörösmarty, J. O. Roads, and C. J. Willmott (2004), Uncertainties in precipitation and their impacts on runoff estimates, *J. Clim.*, 17, 294–304, doi:10.1175/1520-0442(2004)017<0294:UPIATI>2.0.CO;2.
- Flörke, M., and J. Alcamo (2007), Assessment of global scale water stress indicators, in *Global Change: Enough Water for All?*, edited by J. Lozáň, H. Graßl, P. Hupfer, L. Menzel, and C. D. Schönwiese, pp. 200–203, Wiss. Auswertungen und GEO, Hamburg, Germany.
- Fowler, A. (1999), Potential climate change impacts on water resources in the Auckland region (New Zealand), *Clim. Res.*, 11, 221–245, doi:10.3354/cr011221.
- Füssel, H.-M., and J. G. van Minnen (2001), Climate impact response functions for terrestrial ecosystems, *Integr. Assess.*, 2, 183–197, doi:10.1023/A:101327206877.
- Füssel, H. M., F. L. Toth, J. G. van Minnen, and F. Kaspar (2003), Climate impact response functions as impact tools in the tolerable windows approach, *Clim. Change*, 56, 91–117, doi:10.1023/A:1021340513936.
- Gibson, C. A., J. L. Meyer, N. L. Poff, L. E. Hay, and A. Georgakakos (2005), Flow regime alterations under changing climate in two river basins: Implications for freshwater ecosystems, *River Res. Appl.*, 21, 849–864, doi:10.1002/rra.855.
- Gleick, P. H. (1993), *Water in Crisis: A Guide to the World's Fresh Water Resources*, 473 pp., Oxford Univ. Press, New York.
- Global Runoff Data Centre (2008), Long-term mean monthly discharges and annual characteristics of GRDC stations. [http://www.bafg.de/nr\\_267044/GRDC/EN/02\\_Services/02\\_DataProducts/LongTermMonthlyMeans/longtermmonthly\\_node.html?\\_nnn=true](http://www.bafg.de/nr_267044/GRDC/EN/02_Services/02_DataProducts/LongTermMonthlyMeans/longtermmonthly_node.html?_nnn=true), Fed. Inst. of Hydrol., Koblenz, Germany.
- Groffman, P. M., J. S. Baron, T. Blett, A. J. Gold, I. Goodman, L. H. Gunderson, B. M. Levinson, M. A. Palmer, H. W. Paerl, G. D. Peterson, et al. (2006), Ecological thresholds: The key to successful environmental management or an important concept with no practical application?, *Ecosystems*, 9, 1–13, doi:10.1007/s10021-003-0142-z.
- Henrichs, T., B. Lehner, and J. Alcamo (2002), An integrated analysis of changes in water stress in Europe, *Integrated Assessment*, 3, 15–29, doi:10.1076/iaij.3.1.15.7406.
- Hill, W. J., and W. G. Hunter (1966), A review of response surface methodology: A literature survey, *Technometrics*, 8, 571–590.
- Intergovernmental Panel on Climate Change (IPCC) (2000), *Special Report on Emission Scenarios*, 599 pp., Cambridge Univ. Press, Cambridge, U.K.
- Jacob, D. (2001), A note to the simulation of the annual and inter-annual variability of the water budget over the Baltic Sea drainage basin, *Meteorol. Atmos. Phys.*, 77, 61–73, doi:10.1007/s007030170017.
- Jacob, D., et al. (2001), A comprehensive model intercomparison study investigating the water budget during the BALTEX-PIDCAP Period, *Meteorol. Atmos. Phys.*, 77, 19–43, doi:10.1007/s007030170015.
- Kjellström, E., L. Bäring, S. Gollvik, U. Hansson, C. Jones, P. Samuelsson, M. Rummukainen, A. Ullerstig, U. Willén, and K. Wyser (2005), A 140-year simulation of European climate with the new version of the Rossby Centre regional atmospheric climate model (RCA3), *Rep. Meteorol. Climatol.* 108, 54 pp., Swed. Meteorol. and Hydrol. Inst., Norrköping, Sweden.
- Krasovskaja, I., N. W. Arnell, and L. Gottschalk (1994), Flow regimes in northern and western Europe: Development and application of the procedures for classifying flow regimes, in *FRIEND: Flow Regimes From International Experimental and Network Data: Proceedings of the Braunschweig Conference, October 1993*, edited by P. Seuna et al., *IAHS Publ.*, 221, 185–192.
- Kwadijk, J., and J. Rotmans (1995), The impact of climate change on the river Rhine: A scenario study, *Clim. Change*, 30, 397–425, doi:10.1007/BF01093854.
- Laaha, G., and G. Blöschl (2008), A national low flow estimation procedure for Austria, *Hydrol. Sci. J.*, 52, 625–644, doi:10.1623/hysj.52.4.625.
- Lehner, B., and P. Döll (2004), Development and validation of a global database of lakes, reservoirs and wetlands, *J. Hydrol.*, 296, 1–22.
- Limbrick, K. J., P. G. Whitehead, D. Butterfield, and N. Reynard (2000), Assessing the potential impacts of various climate change scenarios on the hydrological regime of the River Kennet at Theale, Berkshire, south-central England, UK: An application and evaluation of the new semi-distributed model, INCA, *Sci. Total Environ.*, 251–252, 539–555, doi:10.1016/S0048-9697(00)00394-6.
- Mansell, M. G. (1997), The effect of climate change on rainfall trends and flooding risk in the west of Scotland, *Nord. Hydrol.*, 28, 37–50, doi:10.2166/nh.1997.003.
- Middelkoop, H., K. Daamen, D. Gellens, W. Grabs, J. C. J. Kwadijk, H. Lang, B. W. A. H. Parmet, B. Schädler, J. Schulla, and K. Wilke (2001), Impact of climate change on hydrological regimes and water resources management in the Rhine Basin, *Clim. Change*, 49, 105–128, doi:10.1023/A:1010784727448.
- Mimikou, M., Y. Koulopoulos, G. Cavadias, and N. Vayianos (1991), Regional hydrological effects of climate change, *J. Hydrol.*, 123, 119–146, doi:10.1016/0022-1694(91)90073-Q.
- Mimikou, M., E. Baltas, E. Varanou, and K. Pantazis (2000), Regional impacts of climate change on water resources quantity and quality indicators, *J. Hydrol.*, 234, 95–109, doi:10.1016/S0022-1694(00)00244-4.
- Mitchell, T. D., and P. D. Jones (2005), An improved method of constructing a database of monthly climate observations and associated high-resolution grids, *Int. J. Climatol.*, 25, 693–712.
- Monk, W. A., P. J. Wood, D. M. Hannah, and D. A. Wilson (2007), Selection of river flow indices for the assessment of hydroecological change, *River Res. Appl.*, 23, 113–122, doi:10.1002/rra.964.
- Myers, R. H. (1999), Response surface methodology—Current status and future directions (including discussion), *J. Qual. Technol.*, 31, 30–74.
- Myers, R. H., A. I. Khuri, and W. H. Carter (1989), Response surface methodology: 1966–1988, *Technometrics*, 31, 137–157.
- Nash, J. E., and J. V. Sutcliffe (1970), River flow forecasting through conceptual models part I—A discussion of principles, *J. Hydrol.*, 10, 282–290, doi:10.1016/0022-1694(70)90255-6.
- Nijssen, B., G. M. O'Donnell, D. P. Lettenmaier, D. Lohmann, and E. F. Wood (2001), Predicting the discharge of global rivers, *J. Clim.*, 14, 3307–3323.
- Olden, J. D., and N. L. Poff (2003), Redundancy and the choice of hydrologic indices for characterizing streamflow regimes, *River Res. Appl.*, 19, 101–121, doi:10.1002/rra.700.
- Pardé, M. (1933), *Fleuves et Rivière*, Collins, Paris.
- Poff, N. L., J. D. Allan, M. B. Bain, J. R. Karr, K. L. Prestegard, B. D. Richter, R. E. Sparks, and J. C. Stromberg (1997), The natural flow regime, *BioScience*, 47, 769–784.
- Postel, S. (1997), *Last Oasis: Facing Water Scarcity*, W. W. Norton, New York.
- Richter, B. D., J. V. Baumgartner, J. Powell, and D. P. Braun (1996), A method for assessing hydrologic alteration within ecosystems, *Conserv. Biol.*, 10, 1163–1174, doi:10.1046/j.1523-1739.1996.10041163.x.

- Siebert, S., P. Döll, J. Hoogeveen, J.-M. Faures, K. Frenken, and S. Feick (2005), Development and validation of the global map of irrigation areas, *Hydrol. Earth Syst. Sci.*, 9, 535–547, doi:10.5194/hess-9-535-2005.
- Smakhtin, V. U. (2001), Low flow hydrology: A review, *J. Hydrol.*, 240, 147–186, doi:10.1016/S0022-1694(00)00340-1.
- Tian, X., A. Dai, D. Yang, and Z. Xie (2007), Effects of precipitation-bias corrections on surface hydrology over northern latitudes, *J. Geophys. Res.*, 112, D14101, doi:10.1029/2007JD008420.
- Tockner, K., and J. A. Stanford (2002), Riverine flood plains: Present state and future trends, *Environ. Conserv.*, 29, 308–330, doi:10.1017/S037689290200022X.
- Ungersböck, M., F. Rubel, T. Fuchs, and B. Rudolf (2001), Bias correction of global daily rain gauge measurements, *Phys. Chem. Earth, Part B*, 26, 411–414.
- United Nations Environment Programme (UNEP) (2002), *Global Environment Outlook 3: Past, Present and Future Perspectives (GEO-3)*, 416 pp., Earthscan, London, U. K.
- United Nations Environment Programme (UNEP) (2007), *Global Environment Outlook: Environment for Development (GEO-4)*, Progress Press, Valetta, Malta.
- van Minnen, J. G., J. Alcamo, and W. Haupt (2000), Deriving and applying response surface diagrams for evaluating climate change impacts on crop production, *Clim. Change*, 46, 317–338.
- Wint, G. R. W., and T. P. Robinson (2007), Gridded livestock of the world 2007, 131 p., Food and Agric. Organ., Rome.
- World Bank (1992), *World Development Report 1992: Development and the Environment*, 308 pp., Oxford Univ. Press, New York.
- Yang, D., D. Kane, Z. Zhang, D. Legates, and B. Goodison (2005), Bias corrections of long-term (1973–2004) daily precipitation data over the northern regions, *Geophys. Res. Lett.*, 32, L19501, doi:10.1029/2005GL024057.

---

J. Alcamo and M. Weiß, Center for Environmental Systems Research, Kurt Wolters Straße, D-34109 Kassel, Germany. (weiss@cesr.de)